Journal of Colloid and Interface Science 644 (2023) 487–495

Contents lists available at ScienceDirect

Journal of Colloid And Interface Science

journal homepage: www.elsevier.com/locate/jcis

Sliding and rolling of yield stress fluid droplets on highly slippery lubricated surfaces

Mattia Carneri [a], Davide Ferraro [a], Afshin Azarpour [b], Alessio Meggiolaro [a], Sebastian Cremaschini [a], Daniele Filippi [a], Matteo Pierno [a], Giuliano Zanchetta [b,*], Giampaolo Mistura [a,*]

[a] Dipartimento di Fisica e Astronomia "G. Galilei", Università di Padova, via Marzolo 8, 35131 Padova, Italy
[b] Dipartimento di Biotecnologie Mediche e Medicina Traslazionale, Università di Milano, via F.lli Cervi 93, 20054 Segrate, Italy

GRAPHICAL ABSTRACT

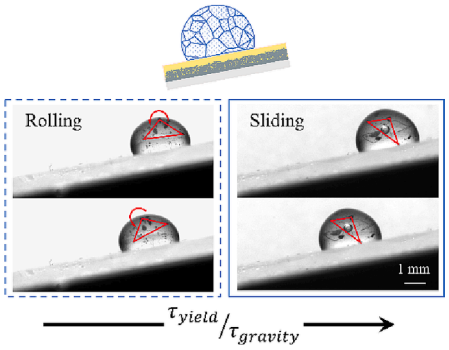

ARTICLE INFO

Keywords:
Yield stress fluids
Wetting
Lubricant infused surfaces
Slip
Surface tension

ABSTRACT

Hypothesis: Droplets of yield stress fluids (YSFs), i.e. fluids that can flow only if they are subjected to a stress above a critical value and otherwise deform like solids, hardly move on solid surfaces due to their high viscosity. The use of highly slippery lubricated surfaces can shed light on the mobility of YSF droplets, which include everyday soft materials, such as toothpaste or mayonnaise, and biological fluids, such as mucus.

Experiments: The spreading and mobility of droplets of aqueous solutions of swollen Carbopol microgels were studied on lubricant infused surfaces. These solutions represent a model system of YSFs. Dynamical phase diagrams were established by varying the concentration of the solutions and the inclination angle of the surfaces.

Findings: Carbopol droplets deposited on lubricated surfaces could move even at low inclination angles. The droplets were found to slide because of the slip of the flowing oil that covered the solid substrate. However, as the descending speed increased, the droplets rolled down. Rolling was favored at high inclinations and low concentrations. A simple criterion based on the ratio between the yield stress of the Carbopol suspensions and the gravitational stress acting on the Carbopol droplets was found to nicely identify the transition between the two regimes.

* Corresponding authors.
E-mail addresses: giuliano.zanchetta@unimi.it (G. Zanchetta), giampaolo.mistura@unipd.it (G. Mistura).

https://doi.org/10.1016/j.jcis.2023.04.075
Received 9 December 2022; Received in revised form 10 April 2023; Accepted 18 April 2023
Available online 22 April 2023

1. Introduction

Wetting is one of the fundamental interfacial phenomena [1], which affects the shape and motion of liquid droplets on solid surfaces and fluid flows in confined geometries [2,3]. It is relevant in a wide range of applications in the biomedical, environmental and energy sectors. The influence of surface chemical composition and roughness has been extensively investigated for Newtonian liquids [4], with particular emphasis on the possibility of controlling wettability and obtaining superhydrophobic surfaces [5], but much less is known for more complex fluids and surfaces. A promising approach to omniphobicity is offered by lubricant-infused surfaces (LIS), made of textured materials imbibed with a low surface tension oil [6,7]. These bioinspired surfaces exhibit various unique properties attributed to their liquid-like and molecularly smooth nature, including excellent liquid repellency, self-healing, anti-icing, anticorrosion, enhanced heat transfer and anti-biofouling [3,8–13]. In particular, they enable low friction droplet motion although the presence of numerous phases, drop, lubricant, solid matrix and vapor, yields a rich tribological scenario [14–18]. Their slippery nature makes them the best candidate for the study of highly viscous non-Newtonian fluids, which barely move on solid surfaces [19]. Then, it is possible to investigate the coupling between dynamic wetting and the rich rheology of soft, structured fluids, such as polymeric solutions, surfactant solutions, gels, or packed microgels, which exhibit viscoelastic behavior in between simple viscous fluids and elastic solids, depending on the probed time scales or the forces at play [20,21]. Indeed, we recently reported an unexpected oscillatory motion of viscoelastic droplets on LIS, despite the homogeneity of the surface and polymeric solution, which can be considered as a sort of novel Weissenberg effect for moving droplets [22].

A particular class of non-Newtonian fluids is represented by yield stress fluids (YSFs), which include everyday soft materials such as toothpaste, shaving foam or mayonnaise, body fluids such as mucus and much harder products such as concrete. Their common feature is that they can flow (that is, deform indefinitely) only if they are subjected to a stress above a critical value; otherwise, they deform in a finite way, like solids [23]. It is rather common that suspensions of dispersed particles in a solvent behave as a yield stress fluid when the volume fraction occupied by the particles is above a critical value [24]. Their closed-packed, amorphous structures are responsible for their rheological behavior: the particles are jammed and can only flow past one another appreciably if a sufficiently high stress, greater than the yield stress, is applied [25]. This threshold can be identified by measuring the stress while applying a continuous shear deformation to the sample at decreasing strain rate: a non-vanishing stress appears for YSFs, which corresponds to a diverging viscosity. However, the motion of a concentrated dispersion depends not only on the bulk flow properties but also on the nature of the confining surfaces.

Aqueous suspensions of swollen Carbopol microgels and aqueous solutions of cross-linked Xanthan polymers are model systems for yield stress fluids, whose rheological properties have been extensively studied [23,25,26]. The flow characteristics of such materials are difficult to predict, as they involve permanently or transiently coexisting solid and liquid regions, which are generally impossible to locate a priori and have been scarcely investigated until recently [27]. Significant slip is observed in the spreading of Carbopol and Xanthan droplets on untreated glass surfaces [28], which is explained in terms of a repulsive electric interaction between the negative polymer chains and the negative surface charges in contact with aqueous solutions due to the dissociation of the terminal silanol groups. After the initial spreading phase, the motion stops and a mechanical equilibrium is reached, characterized by a stable contact angle. Contrary to what is observed with Newtonian fluids and what is expected from classical thermodynamics, the final contact angle increases with the size of Carbopol droplets [29]. If the spreading of a droplet occurs on a thin film of the same material, the Carbopol droplet reaches a final equilibrium shape once the driving stresses inside the droplet fall below the yield stress [30], in contrast to a Newtonian droplet that spreads continuously until a completely flat film is formed. If a YSF droplet is placed on a dry superhydrophobic surface, the resulting adhesive stress is similar in magnitude to the gravitational and yield stresses. This allows the motion of Xanthan droplets descending an inclined superhydrophobic surface to be clearly differentiated in pure rolling, sliding and sticking by varying the surface inclination and Xanthan concentration [31]. Spreading LISs, in which the lubricant impregnates the surface micro-textures and covers them, can be designed to allow the mobility of the yield stress fluids that would otherwise be immobile under the same flow conditions [32]. For example, Carbopol droplets, which are found to adhere to both flat hydrophobic and patterned superhydrophobic surfaces, move readily on a spreading LIS impregnated with silicone oil. In other words, a spreading LIS acts as a stable Newtonian lubricating layer with an effective viscosity that depends on the viscosity of the lubricating fluid and the aspect ratio of the microtexture. However, the nature of the motion of YSF droplets, for example, whether they slide or roll down from an inclined surface, has hardly been explored in the literature. The aim of this work is to fill this gap by providing a comprehensive picture of the mobility of YSF droplets on slippery lubricated surfaces within a wide range of yield stress values.

2. Materials and methods

2.1. Lubricant infused surfaces (LIS)

As slippery surfaces, we prepared hybrid substrates formed by glass slides coated with a LIS. Standard glass microscope slides were cleaned with common detergents and rinsed in acetone and purified water baths. A $\sim$ 25 μm thick porous polytetrafluoroethylene (PTFE) membrane (Sterlitech Corporation) was placed on one face of the slide and wetted with ethanol: the evaporation of ethanol leads to capillary adhesion of the membrane to the slide [33]. With a dip coater (Kibron Inc. LayerX 274), the membrane attached to the slide was then infused with fluorinated oil (Fomblin PFPE Perfluoropolyether Y LVAC 06/6) having a viscosity of 120 mPa s at $T = 20\ ^{\circ}C$, using the procedure reported in [18]. To ensure a controlled thickness of the liquid layer above the membrane of about 0.5 μm, the withdrawal velocity was set at 0.12 mm/min, see reference [22] for more details.

2.2. Yield stress fluids

Different yield stress fluids, based on swollen microgels, were prepared and characterized. Namely, we studied two aqueous solutions of the polyacrylic acid Carbopol Aqua SF2 and Carbopol 971P NF (Lubrizol) at different polymer mass fractions. The two families differ in their typical microgel radius (about 0.25 and 2 μm, respectively) and in their yield stress values as a function of concentration [34]. Carbopol Aqua SF2 (SF2) samples were diluted to the final concentration in MilliQ water, from a concentrated batch solution at low pH. The pH gradually increased by adding drops of NaOH 10 M; around pH 7, the microgels swell and the solution becomes fully transparent, developing a yield stress above a concentration of approximately 0.2% [35]. Carbopol 971P NF (971P) is available in powder form. It was dispersed in MilliQ water at the final concentration. The pH of the solution was increased to 7 by adding drops of NaOH 10 M, resulting in a fully transparent yield stress fluid above 0.05% [36]. All samples were gently mixed for several days and the pH was monitored and adjusted to obtain homogeneous suspensions that allow imaging of internal tracers [36]. The density ρ of all the investigated solutions was close to that of water, while there are no reliable measurements of the surface tension γ of Carbopol suspensions reported in the literature [30]. We tried to measure it directly with the pendant drop method [37], but the droplet curvature, and therefore the derived γ, varied considerably over time and depended on the infusion rate; as a result, we obtained values within the range 48–68

mN/m. Consequently, droplets are expected to be cloaked by a thin lubricant film once they are deposited on silicone or fluorinated oil lubricated surfaces [14,38]. Finally, pure glycerol was used as a Newtonian reference for the motion of droplets on slippery lubricated surfaces.

The rheological tests of the YSF solutions were performed on a commercial rheometer (MCR 302, Anton Paar GmbH) using a cone and plate geometry with a cone radius and angle of 25 mm and 1°, respectively. The temperature was kept at 22 °C with a Peltier element. Fresh samples were loaded for each series of experiments and reproducibility was verified by repeating a single test several times. Samples were pre-sheared at high shear rates for hundreds of seconds and then left to rest for a similar time to guarantee reproducible and time independent behavior. From oscillatory experiments at $\omega = 1$ rad/s at increasing amplitudes in the range of 0.1–400%, we estimated the limits of the linear viscoelastic regime; we then extracted the linear viscoelastic properties from small-amplitude oscillatory shear experiments in the frequency range $\omega = 0.1$–100 rad/s at strain $\gamma = 1\%$. To estimate the yield stress τ_{yield}, flow curve tests were performed by applying a constant strain rate, decreasing from 100 to 0.01 s^{-1}, using logarithmically increasing sampling times to guarantee steady state conditions at all shear rates. Data below 0.1 s^{-1} s were not considered, as they often revealed the appearance of slip at the interface. The stress data, shown in Fig. 1, were fitted according to the three-component (TC) model [39], which provides both a clearer physical insight and a better description of the experimental data than the Herschel–Bulkley model [23]. However, the yield stress estimates of the two models and their dependence on concentration were always consistent. As reported in Table 1, for both Carbopol samples τ_{yield} increases roughly linearly with concentration in the investigated ranges; a similar dependence is observed for the low-frequency elastic modulus G.

2.3. Optical setup

To monitor the motion of the droplets on the LIS, we used the optical setup shown in Fig. 2 [40]. A rotating stage controlled by a computer could change the angle of inclination with respect to the horizontal α of the lubricated substrate with 0.5° precision. A vertical syringe pump was mounted on an X-Y table. In this way, it was possible to dose droplets of known volume Ω in the range between 10 and 40 μl on a well-defined position of the substrate. To favor drop detachment, a short silicone tubing was attached to the tip of the stainless-steel needle. To minimize inertial effects, we slowly extruded the droplets onto the surface and placed the tubing tip 2 mm above the LIS. The lateral profile of the drop was viewed using a CMOS camera (BASLER acA800-510um) mounted along the rotation axis of the stage and equipped with a macro zoom lens (LINOS MeVis C 50 mm/f 1.8). To enhance the optical contrast, the droplet was backlighted with a white LED source. Movies of the drop motion were acquired at sample rate intervals between 100 and 2000 fps and analyzed using a custom-made LabVIEW script.

Table 1
Main rheological properties of the Carbopol yield stress fluids.

Concentration	τ_{yield}(Pa)	G (Pa)
Carbopol SF2		
0.25 wt%	0.2±0.1	3±1
0.50 wt%	0.6±0.1	8±1
0.75 wt%	0.7±0.1	10±1
1.00 wt%	1.2±0.1	15±1
Carbopol 971P		
0.10 wt%	0.6±0.1	5±1
0.30 wt%	3.8±0.1	25±2
0.40 wt%	4.2±0.1	27±2
0.50 wt%	6.7±0.1	44±2
0.70 wt%	7.9±0.1	48±2
1.00 wt%	10.8±0.1	66±2

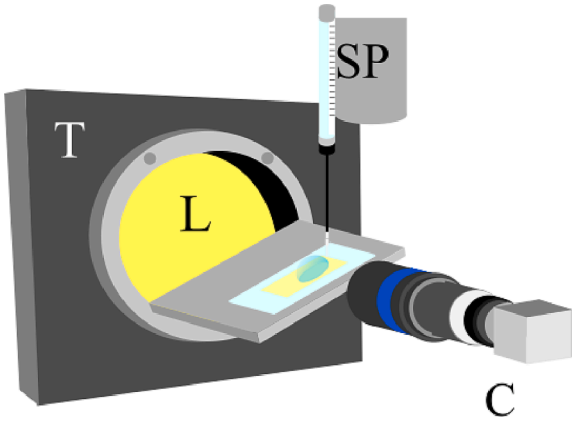

Fig. 2. Optical setup: T = tilter, L = LED source, SP = syringe pump, C = camera.

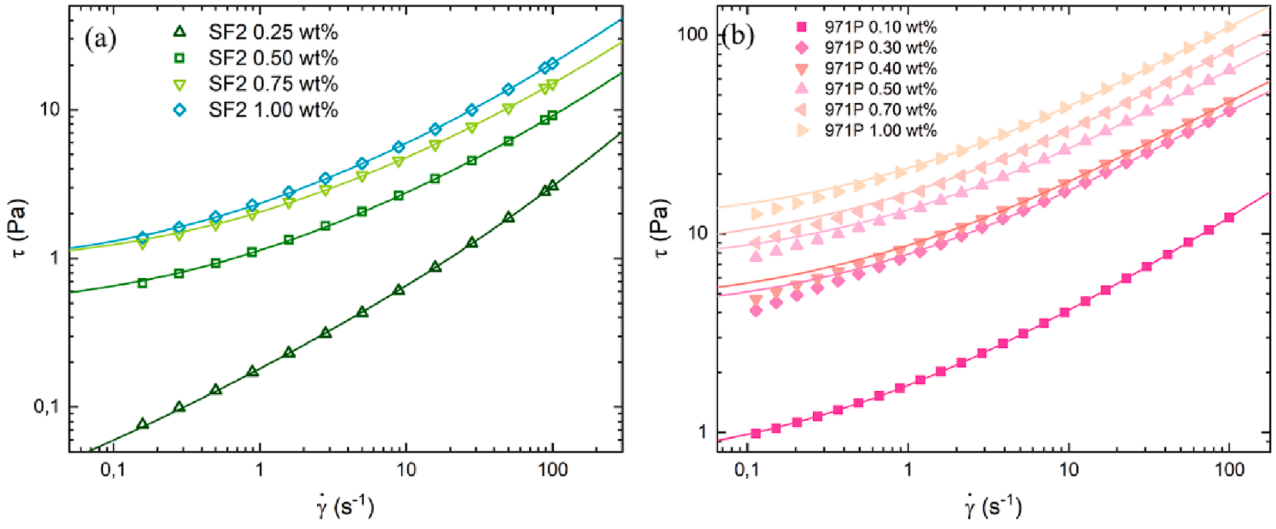

Fig. 1. Shear stress τ vs. shear strain $\dot{\gamma}$ curves of Carbopol SF2 (a) and 971P (b) solutions on a log–log scale. The continuous curves show the corresponding three-component (TC) fits.

3. Results

3.1. Droplet spreading

Fig. 3 shows the time evolution of the droplet profile as derived from video recordings of the formation and deposition of droplets of volume $\Omega = 20$ µl on a horizontal LIS, see also supplementary video S1. We carried out preliminary tests using droplets of volume equal to 10, 20, 30 e 50 µl and we did not observe significant changes in their motion. We chose to work with 20 µl droplets because the motion was highly reproducible and it was possible to study it over an ample range of inclination angles, with the droplet occupying a small fraction of the camera frame size (droplet radius of ~ 1.5 mm with respect to a frame size of ~ 15 mm). Furthermore, the overall shape was that of a hemisphere determined by interfacial tension and not flattened by gravity. The opposite limit of large drops (puddles) will be the subject of a dedicated study. The graph in Fig. 3(a) indicates the diameter D of the wetted surface, together with some representative snapshots of the initial and final profiles, while Fig. 3(b) reports the corresponding contact angle θ. The initial time corresponds to the detachment of the droplet from the needle at the completion of the infusion process, which typically takes a few seconds. In the case of glycerol, the droplets reach the final configurations almost instantaneously. Instead, droplets of both Carbopol suspensions exhibit a slow but significant expansion of the wetted area, accompanied by a decrease in the contact angle: in the case of SF2 0.50 wt%, the relative increase in D is greater than 10% over 5 min. Varying the syringe flow rate between 0.06 and 0.54 ml/min did not produce any significant variation. In all experiments presented in the following, the extrusion flow rate was 0.3 ml/min, comparable to that used in a recent study [30].

The spreading of Carbopol droplets depends on their concentration, as shown in Fig. 4(a) and (b). Interestingly, the two types of Carbopol present significant differences. In the case of SF2, the pronounced variation observed in D is related to the corresponding decrease in θ as the solution becomes more concentrated. Actually, the continuous lines in Fig. 4(a) represent the diameter of the area wetted by a hemispherical cap of volume Ω and an instantaneous contact angle θ for selected Carbopol concentrations [41]. In the beginning, the lines lie below the corresponding experimental data, but eventually they nicely overlap, suggesting that the initial shape assumed by the SF2 droplets is somewhat peaked and slowly relaxes to that of a perfect hemisphere. The good agreement between the experimental data and the geometrical calculations [41] implies that the observed phenomenology is mainly an interfacial effect: SF2 droplets spread until the contact line becomes pinned by surface tension, with D reaching different final values as a result of the different contact angles. A quite distinct behavior is observed in the case of 971P droplets. The three solutions have the same θ, yet D decreases significantly with concentration, suggesting that its dependence is primarily rheological. Indeed, this behavior is similar to that reported in the spreading of Carbopol drops over a thin film of the same material, where, as the yield stress increases, the final radius becomes correspondingly smaller [30]. This can be explained by assuming that the spread of a droplet, yielding under the effect of capillary and gravitational stresses, stops as they fall below the yield stress τ_{yield}.

Apart from these differences, for both types of solution, the time constant t_f required to reach the final configuration decreases with concentration: for example, t_f is equal to approximately 5 min for SF2 0.25 wt% and drops to 30 s for SF2 1 wt%. Furthermore, t_f is significantly shorter for 971P droplets: for 971P 0.10 wt% ($\tau_{yield} = 0.63$ Pa), t_f is approximately 10 s, while for SF2 0.50 wt%, possessing a similar threshold value ($\tau_{yield} = 0.60$ Pa), t_f is approximately 50 s.

3.2. Droplet motion

We have then studied the gravity induced motion of Carbopol droplets on inclined surfaces. Fig. 5 shows a representative set of consecutive measurements of SF2 0.25 wt% droplets deposited manually with a micropipette on a LIS inclined by an angle $\alpha = 3°$ (empty symbols). The curves represent the temporal dependence of the front contact point of the descending droplets having $\Omega = 20$ µl. Clearly, the data show a set of quite different, non-linear curves that reflect the simultaneous relaxation processes following droplet generation and deposition, as discussed in the previous section. To remove this artifact, droplets generated with the syringe pump were gently deposited on a horizontal LIS. After a sufficiently long time to allow complete stop of the spreading process, the LIS was quickly tilted to the same $\alpha = 3°$ and the droplet motion was recorded. The resulting curves are indicated as full symbols in Fig. 5. The straight lines indicate a viscosity dominated motion, as expected [16,42]. Small variations in their slope, <5%, can be taken as the degree of reproducibility of these measurements. All the measurements discussed in the rest of the section were taken following the latter procedure. We have considered only $\alpha \geq 3°$ because, for smaller angles, the motion becomes very slow (velocity below approximately 0.01 mm/s) and the results may be affected by droplet

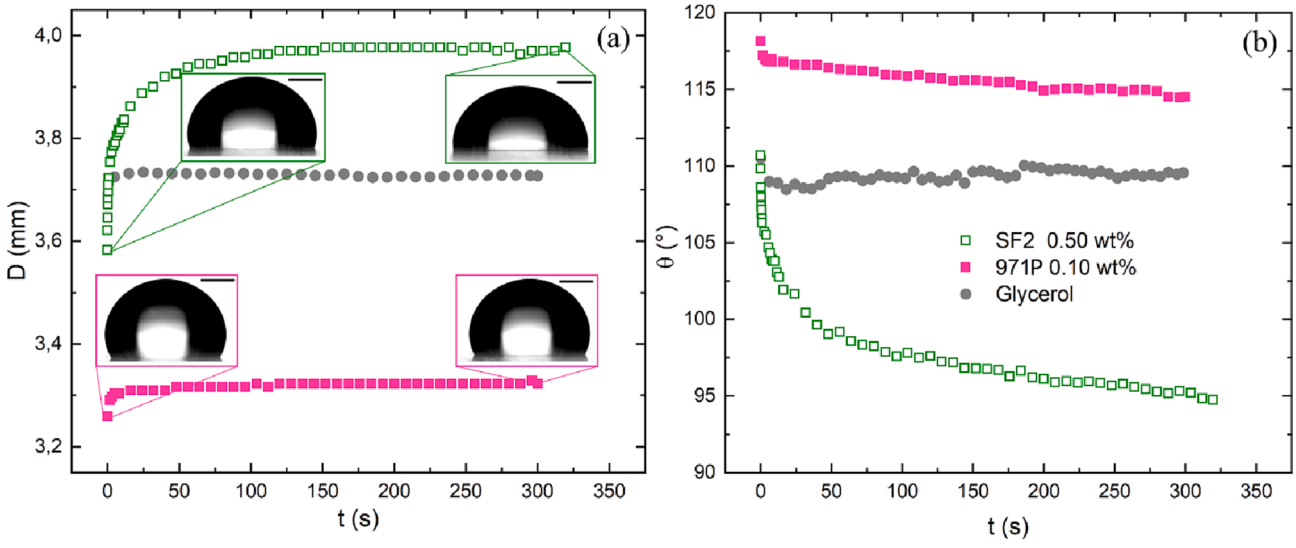

Fig. 3. Temporal variation of the diameter D of the wetted area (a) and the corresponding contact angle θ (b) of different droplets of volume 20 µl deposited on a horizontal LIS. The scale bar of the four representative snapshots of the droplet contour is 1 mm.

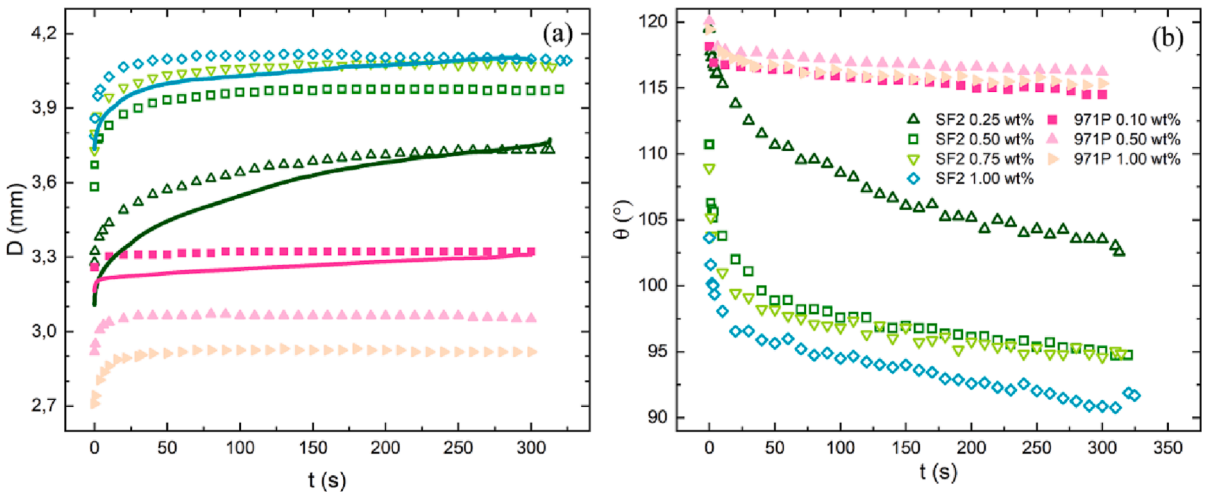

Fig. 4. Temporal variation of the diameter D of the contact line (a) and the contact angle θ (b) of Carbopol drops at different concentrations and volume 20 μl deposited on a horizontal LIS. The continuous lines are the diameters of the wetted areas of hemispherical caps derived from the corresponding contact angles, as explained in the text.

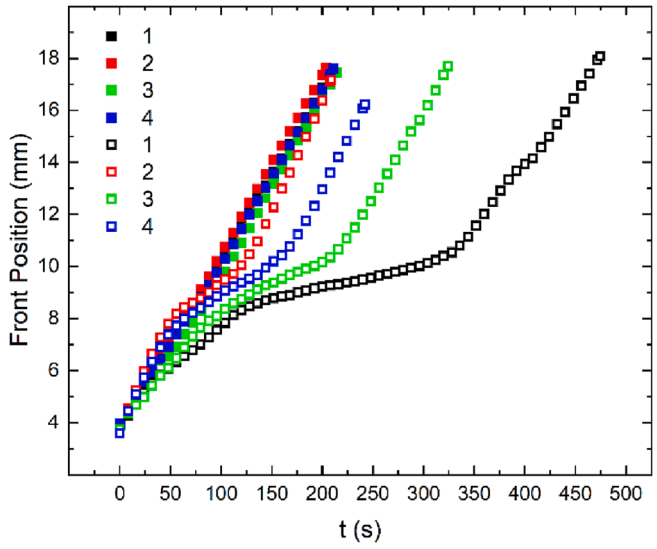

Fig. 5. Time evolution of the front position of the contact line of four consecutive droplets of SF2 0.25 wt% with volume $\Omega = 20$ μl deposited on lubricated surfaces inclined by $\alpha = 3°$. Empty symbols represent the motion of droplets deposited manually with a micropipette on the already tilted surface. The full symbols refer to droplets deposited on the horizontal surface using a syringe pump; after spreading, the surface is quickly tilted to $\alpha = 3°$ and the resulting droplet descent motion is recorded.

evaporation. Actually, the height of the YSF droplets decreases by about 10% over 10 min, the minimum time required for the droplet to cover the length of the slide at $\alpha < 3°$.

At low inclinations, Carbopol droplets are found to slide: the selected snapshots of Fig. 6(a), which refer to a droplet of 971P 0.50 wt% and volume $\Omega = 20$ μl descending a lubricated surface inclined by an angle $\alpha = 10°$, and the accompanying supplementary video S2 clearly show a downward displacement of the droplet but no relative movement of the trapped tracers. If instead α is increased above 20°, the droplets not only move faster, as expected, but also change the nature of the motion to rolling as shown in Fig. 6(b) and the supplementary video S3, which correspond to $\alpha = 45°$: representative triangles that join three tracers rotate over time. From introductory mechanics, it is well known that a rigid sphere rolls down a rough inclined plane, while a rigid cube slides down it. In the case of a liquid drop, a variety of motions becomes possible because a deformable body maintains contact with the surface over a finite area [43], which have been theoretically analyzed in detail for the simple case of two-dimensional droplets [44–46]. For a viscous droplet, two distinct motions are typically observed. A nonwetting droplet on a superhydrophobic surface rolls down [47,48] while, if the droplet partially wets a solid surface, it slides along it [49–51]. In the case of slippery lubricated surfaces, all studies of partially wetting Newtonian droplets indicate only rolling motion on LIS [14–16]. Carbopol droplets moving on LIS can instead undergo either sliding or rolling, depending on initial conditions such as Ω and α. Interestingly, low-concentration Carbopol droplets on lubricated surfaces exhibit the standard behavior observed with Newtonian droplets on LIS [14–16], that is, they roll down. For example, Fig. 6(c) and the supplementary video S4 refer to droplets of 971P 0.10 wt% that descend from a LIS inclined to $\alpha = 10°$. If we compare this sequence of snapshots with that of Fig. 6(a), we clearly see that the less concentrated droplets not only move much faster (about a factor 30) due to their lower viscosity but also roll and do not slide. In summary, experimental evidence suggests that the change from sliding to rolling is a peculiar property of YSF droplets descending slippery surfaces. A somewhat similar behavior was reported in the case of much larger YSF drops, $\Omega = 250$ μl, made of Xanthan gum and descending a dry superhydrophobic surface [31]: sliding was observed at low inclinations, followed by rolling at higher α. Surprisingly, concentrated Xanthan droplets were pinned to superhydrophobic surfaces inclined to angles greater than ~ 10°, while water droplets are very mobile on these surfaces: droplets as small as 1 μl easily roll down at inclinations of 1°. Instead, on lubricated surfaces, the sliding speed of YSF droplets with $\Omega = 20$ μl is comparable to that found with much larger drops, $\Omega = 250$ μl, on dry superhydrophobic surfaces, a clear indication that LISs are much more slippery than superhydrophobic dry rough surfaces, ideal for the study of viscous non-Newtonian droplets. Indeed, this is also confirmed by the sliding of drops made of shear-thinning polymers in the absence of yield stress [22].

The dynamical phase diagrams shown in Fig. 7 summarize the different types of motion exhibited by the descending droplets of the 971P and SF2 solutions, as the Carbopol concentration and the angle of inclination α vary. In the case of 971P droplets, as α increases, sliding is first observed, followed by rolling. Rolling is favored at high inclinations and low concentrations. Interestingly, the analogous phase diagram of SF2 droplets exhibits only rolling, in agreement with previous studies of Newtonian droplets on LISs. Next, we discuss these two regimes in more detail.

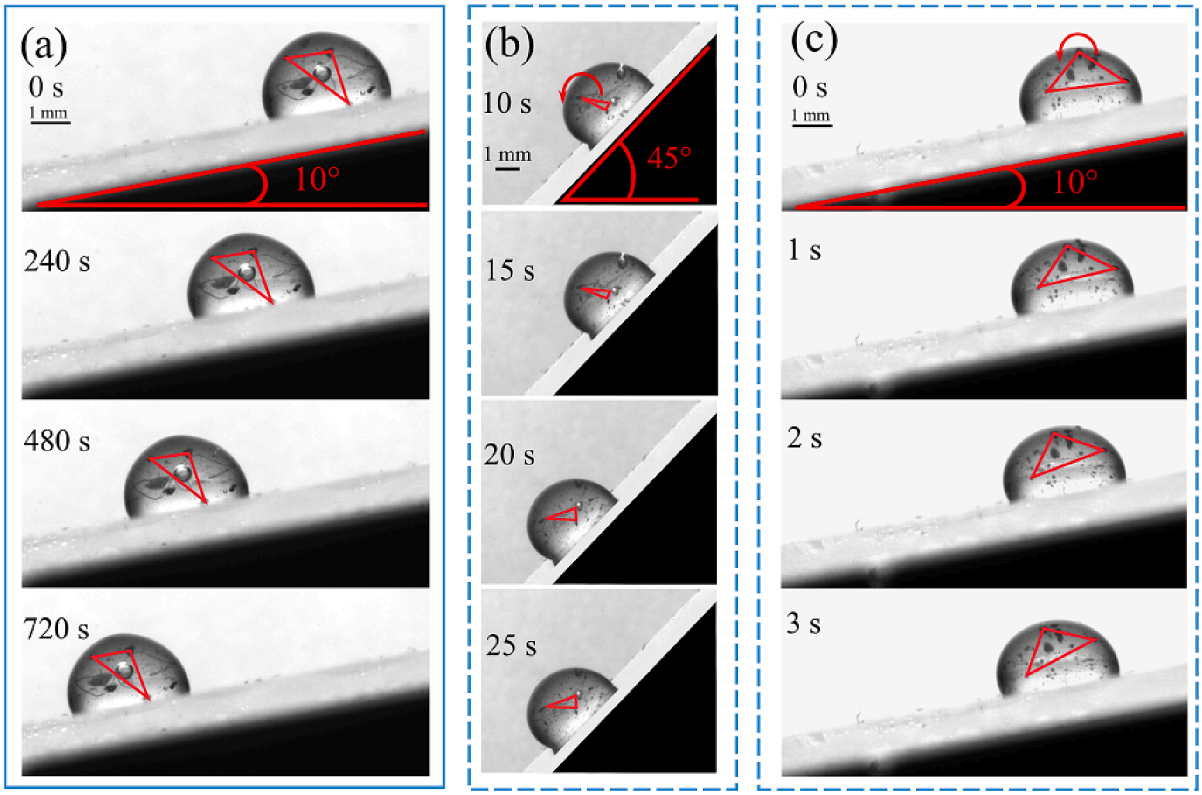

Fig. 6. Snapshots of (a) sliding and (b) rolling of droplets of 971P 0.50 wt%: at 10° inclination, the air bubbles in the droplet show no relative motion inside of the droplet, indicating a sliding motion (see also the supplementary movie S2); at 45° inclination, the red triangle rotates indicating the rolling motion of the droplet (see also the supplementary movie S3). (c) Snapshots of droplets of 971P 0.10 wt% showing rolling at an inclination angle of 10° (see also the supplementary movie S4). All droplets have volume $\Omega = 20$ μl. (For interpretation of the references to colour in this figure legend, the reader is referred to the web version of this article.)

We first focus on the sliding regime, in which the 971P droplets do not undergo any shear. Fig. 8 shows that the sliding droplets move downward with a steady velocity U that is proportional to sinα for two representative 971P solutions, indicative of a typical Stokes behavior regulated by a constant viscosity and where U is due to the flow of the oil film that covers the filter. Consequently, we model the system as a solid droplet moving with velocity U separated by an oil film of thickness h from the filter, as schematically pictured in the inset of Fig. 8. Given the expected small value of h, the flow profile in the oil film is $u(z) = Uz/h$, which yields a shear stress at the oil-droplet boundary $\tau_{zx} = \mu_{oil}U/h$, where μ_{oil} is the oil viscosity. In stationary conditions, τ_{zx} must be equal to the gravitational stress $\tau_{grav} = b\rho g sin\alpha$, where b is the maximum height of the droplet having density ρ deposited on a LIS inclined by an angle α, and g is the acceleration of gravity [31]. A linear fit to the sliding data in Fig. 8 provides an estimate of the oil film thickness $h \sim 0.3$ μm, in agreement with the value derived from dip coating. The fact that h is much larger than the intrinsic slip length of a few nm measured for Carbopol flowing past a solid wall [25] confirms that the sliding of the 971P droplets is dominated by the slip caused by the flowing oil. This conclusion also agrees with the results of recent bulk experiments carried out with a conventional rheometer where Carbopol is confined between a flat plate and a spreading LIS [32]. The fact that, in the zoom of Fig. 8(b), the 971P 1.0 wt% datapoints at high inclinations lie well above the extrapolated straight line may be an indication that at these

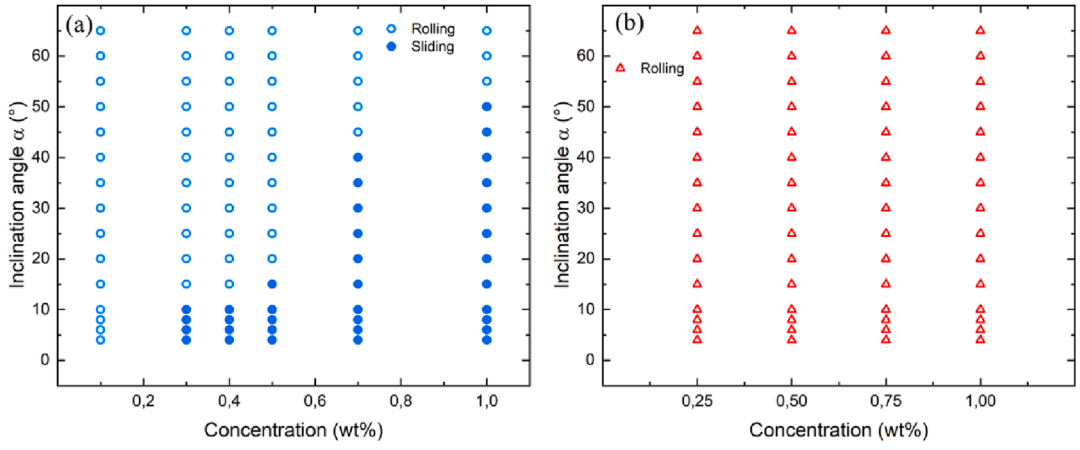

Fig. 7. Dynamical phase diagrams of 971P (a) and SF2 (b) droplets at different concentrations moving on lubricated surfaces at different angles of inclination. The droplets have volume $\Omega = 20$ μl.

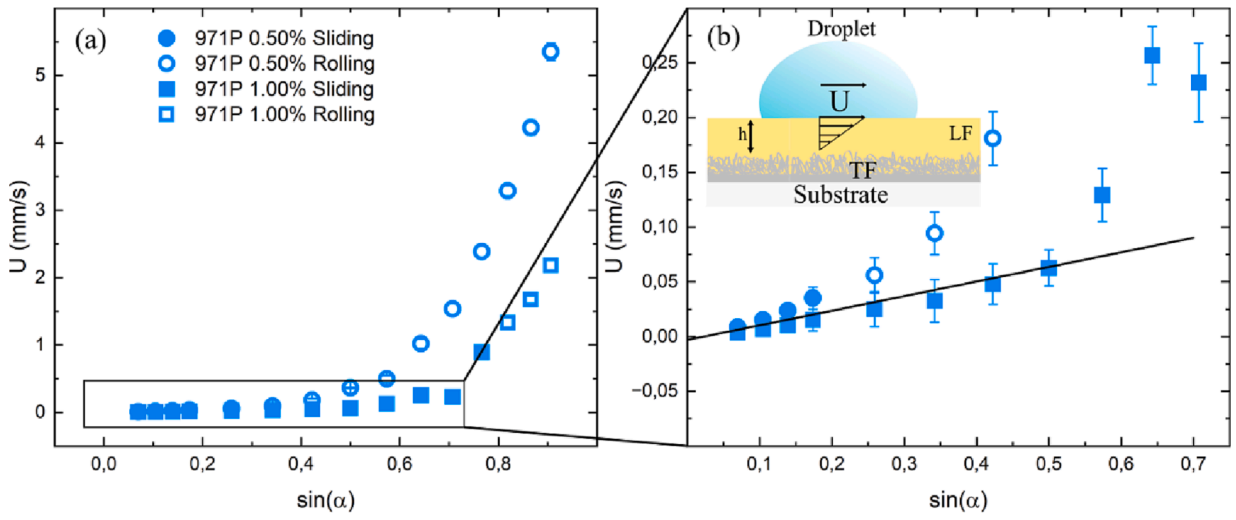

Fig. 8. (a) Steady velocity of droplets of 971P at two different concentrations descending lubricated surfaces at different angles of inclination. The droplets have volume $\Omega = 20$ µl. (b) Enlargement of the data enclosed in the rectangular box. The inset shows a pictorial view of the interface between a droplet sliding with velocity U on a lubricant film LF of thickness h coating a Teflon filter TF infused with the same lubricant. This lubricant infused surface covers the glass slide S.

velocities, and thus shear stresses, wall slip also contributes to the overall droplet velocity [52].

We now analyze under what conditions Carbopol droplets roll. In a recent investigation of the mobility of Xanthan drops on dry superhydrophobic surfaces, it was argued that the ratio of yield and gravitational stresses τ_{yield}/τ_{grav} differentiates the rolling and sliding regimes. In detail, when the gravitational stress overcomes the yield stress, the drop is fluidized at least in its lower part in contact with the lubricated surface and thus rolls down on a slippery surface. Analogously, we rescaled the data in Fig. 7 in the new phase diagram shown in Fig. 9, where the two types of motion are classified in terms of the yield stress τ_{yield} of the various solutions as measured from the bulk rheology, normalized to the corresponding gravitational stress τ_{grav}. The criterion originally proposed for rolling of YSF droplets on dry superhydrophobic surfaces [31] is also found to be well satisfied on lubricated surfaces: in the case of SF2 droplets, all the explored conditions are characterized by $\tau_{yield}/\tau_{grav} < 1$ while 971P droplets undergo rolling when $\tau_{yield}/\tau_{grav} < 1$. Such a good agreement is somewhat surprising considering the higher complexity of the interface, where there is both slip in the oil film and shear of the YSF [32]. Conversely, sliding of 971P droplets is found for τ_{yield}/τ_{grav} greater than 1. In this case, sliding is also observed in a intermediate area colored in gray extending somewhat below 1 and is not unexpected given the simplicity of this argument. Actually, we did not imagine that this criterion, which compares the bulk rheology of the Carbopol suspensions (τ_{yield}) to the experimental conditions (Ω and α), worked so remarkably well to account for our measurements. Further information may come from high-resolution, local imaging of the bottom layers of the sliding/rolling droplets.

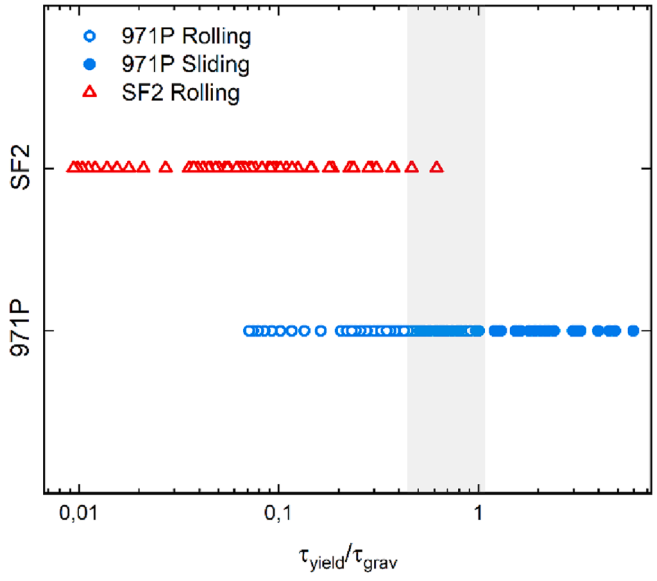

Fig. 9. Phase diagram in which the type of droplet motion is classified in terms of the ratio τ_{yield}/τ_{grav} for droplets of 971P and SF2 solutions.

4. Conclusions

We studied the dynamic wetting on an engineered substrate focusing on both spreading and mobility of a yield stress fluid based on a suspension of swollen Carbopol microgels. By changing their concentration [23,35], it was possible to vary their bulk yield stress τ_{yield}, that is the minimum stress required to fluidize the suspension. The characterization of the mobility of Carbopol droplets on an inclined plane was only made possible by the use of lubricant infused surfaces [22,32]. Indeed, we report for the first time that millimeter-size YSF droplets show distinct sliding and rolling regimes on such slippery surfaces. Sliding occurs when the droplets are more solid-like, and their velocity is determined by the shear flow of the oil film that covers the solid substrate. Instead, when the gravitational stress exceeds a certain threshold, the droplet is partially fluidized and can thus deform and roll down, as generally reported for ordinary Newtonian droplets [14–16]. A simple criterion based on the ratio τ_{yield}/τ_{grav} was found to capture the transition between the two regimes: rolling when $\tau_{yield}/\tau_{grav} \lesssim 1$ and sliding when $\tau_{yield}/\tau_{grav} \gtrsim 1$. Such a scaling could be used as a reliable gauge in the design of microfluidic devices that involve the control of the motion of YSF droplets. Particle imaging velocimetry of dispersed tracers [28], integrated by dedicated numerical simulations [30,53], can provide further useful insight into the local rearrangements at the oil-YSF interface and the extent of fluidization within sliding/rolling droplets.

Our results confirm that the study of the gravity induced motion of droplets on slippery lubricated surfaces can provide a simple but powerful tool to address the interfacial and bulk properties of a wide range of complex fluids, such as colloidal suspensions or polymeric solutions. Surprisingly, these fluids would barely move on superhydrophobic dry rough surfaces, which are known to present very little friction to the motion of water droplets [54,55], but that, however, lose

some of their useful characteristics when exposed to complex fluids [31,56].

Data Availability

Data will be made available on request.

CRediT authorship contribution statement

Mattia Carneri: Methodology, Visualization, Data curation. **Davide Ferraro:** Methodology, Software, Validation. **Afshin Azarpour:** Methodology. **Alessio Meggiolaro:** Methodology, Software. **Sebastian Cremaschini:** Methodology. **Daniele Filippi:** Methodology, Software. **Matteo Pierno:** Methodology, Visualization, Funding acquisition. **Giuliano Zanchetta:** Conceptualization, Methodology. **Giampaolo Mistura:** Conceptualization, Project administration, Supervision.

Declaration of Competing Interest

The authors declare that they have no known competing financial interests or personal relationships that could have appeared to influence the work reported in this paper.

Data availability

Data will be made available on request.

Acknowledgements

The authors are particularly grateful to Tommaso Bellini for useful discussions, and Giorgio Delfitto and Paolo Sartori for their valuable technical assistance. The partial funding from PRIN2017 UTFROM of the Italian Ministry of University and Research and from the University of Padova through the STARS grant EXODROP and the BIRD grant 2021 BiodivSeq is kindly acknowledged.

Appendix A. Supplementary material

Supplementary data to this article can be found online at https://doi.org/10.1016/j.jcis.2023.04.075.

References

[1] P.G. De Gennes, F. Brochard-Wyart, D. Quéré, Capillarity and Wetting Phenomena: Drops, Bubbles, Pearls, Waves, Springer, New York, 2004.
[2] L. Bocquet, E. Charlaix, Nanofluidics, from bulk to interfaces, Chem. Soc. Rev. 39 (3) (2010) 1073–1095.
[3] G. Mistura, M. Pierno, Drop mobility on chemically heterogeneous and lubricant-impregnated surfaces, Adv. Phys.-X 2 (2017) 591–607.
[4] D. Bonn, J. Eggers, J. Indekeu, J. Meunier, E. Rolley, Wetting and spreading, Rev. Mod. Phys. 81 (2009) 739–805.
[5] P. Roach, N.J. Shirtcliffe, M.I. Newton, Progess in superhydrophobic surface development, Soft Matter 4 (2) (2008) 224–240.
[6] A. Lafuma, D. Quere, Slippery pre-suffused surfaces, EPL 96 (2011) 56001.
[7] T.-S. Wong, S.H. Kang, S.K.Y. Tang, E.J. Smythe, B.D. Hatton, A. Grinthal, J. Aizenberg, Bioinspired self-repairing slippery surfaces with pressure-stable omniphobicity, Nature 477 (2011) 443–447.
[8] S. Anand, A.T. Paxson, R. Dhiman, J.D. Smith, K.K. Varanasi, Enhanced Condensation on Lubricant-Impregnated Nanotextured Surfaces, ACS Nano 6 (11) (2012) 10122–10129.
[9] M.J. Kreder, J. Alvarenga, P. Kim, J. Aizenberg, Design of anti-icing surfaces: smooth, textured or slippery? Nat. Rev. Mater. 1 (1) (2016) 15003.
[10] D.C. Leslie, A. Waterhouse, J.B. Berthet, T.M. Valentin, A.L. Watters, A. Jain, P. Kim, B.D. Hatton, A. Nedder, K. Donovan, E.H. Super, C. Howell, C.P. Johnson, T.L. Vu, D.E. Bolgen, S. Rifai, A.R. Hansen, M. Aizenberg, M. Super, J. Aizenberg, D.E. Ingber, A bioinspired omniphobic surface coating on medical devices prevents thrombosis and biofouling, Nat. Biotechnol. 32 (11) (2014) 1134–1140.
[11] J.S. Li, E. Ueda, D. Paulssen, P.A. Levkin, Slippery lubricant-infused surfaces: properties and emerging applications, Adv. Funct. Mater. 29 (2019) 1802317.
[12] D.P. Regan, C. Howell, Droplet manipulation with bioinspired liquid-infused surfaces: A review of recent progress and potential for integrated detection, Curr. Opin. Colloid Interface Sci. 39 (2019) 137–147.
[13] J. Wang, L. Wang, N. Sun, R. Tierney, H. Li, M. Corsetti, L. Williams, P.K. Wong, T. S. Wong, Viscoelastic solid-repellent coatings for extreme water saving and global sanitation, Nat. Sustain. 2 (12) (2019) 1097–1105.
[14] J.D. Smith, R. Dhiman, S. Anand, E. Reza-Garduno, R.E. Cohen, G.H. McKinley, K. K. Varanasi, Droplet mobility on lubricant-impregnated surfaces, Soft Matter 9 (6) (2013) 1772–1780.
[15] D. Daniel, J.V.I. Timonen, R.P. Li, S.J. Velling, J. Aizenberg, Oleoplaning droplets on lubricated surfaces, Nat. Phys. 13 (10) (2017) 1020–1025.
[16] A. Keiser, L. Keiser, C. Clanet, D. Quere, Drop friction on liquid-infused materials, Soft Matter 13 (39) (2017) 6981–6987.
[17] C. Rigoni, D. Ferraro, M. Carlassara, D. Filippi, S. Varagnolo, M. Pierno, D. Talbot, A. Abou-Hassan, G. Mistura, Dynamics of ferrofluid drops on magnetically patterned surfaces, Langmuir 34 (30) (2018) 8917–8922.
[18] P. Sartori, E. Guglielmin, D. Ferraro, D. Filippi, A. Zaltron, M. Pierno, G. Mistura, Motion of Newtonian drops deposited on liquid-impregnated surfaces induced by vertical vibrations, J. Fluid Mech. 876 (2019) R4.
[19] S. Varagnolo, D. Filippi, G. Mistura, M. Pierno, M. Sbragaglia, Stretching of viscoelastic drops in steady sliding, Soft Matter 13 (17) (2017) 3116–3124.
[20] J.D. Ferry, Viscoelastic properties of polymers, 3rd ed.,, John Wiley and Sons, Inc., 1980.
[21] G. Zanchetta, S. Mirzaagha, V. Guida, F. Zonfrilli, M. Caggioni, N. Grizzuti, R. Pasquino, V. Trappe, Colloidal fibers as structurant for worm-like micellar solutions, Colloid Polym. Sci. 296 (2018) 1379–1385.
[22] P. Sartori, D. Ferraro, M. Dassie, A. Meggiolaro, D. Filippi, A. Zaltron, M. Pierno, G. Mistura, Oscillatory motion of viscoelastic drops on slippery lubricated surfaces, Commun. Phys. 5 (1) (2022).
[23] P. Coussot, Yield stress fluid flows: A review of experimental data, J. Nonnewton. Fluid Mech. 211 (2014) 31–49.
[24] R. Borrega, M. Cloitre, I. Betremieux, B. Ernst, L. Leibler, Concentration dependence of the low-shear viscosity of polyelectrolyte micro-networks: From hard spheres to soft microgels, Europhys. Lett. 47 (1999) 729–735.
[25] S.P. Meeker, R.T. Bonnecaze, M. Cloitre, Slip and flow in soft particle pastes, Phys. Rev. Lett. 92 (2004), 198302.
[26] P. Coussot, L. Tocquer, C. Lanos, G. Ovarlez, Macroscopic vs. local rheology of yield stress fluids, J. Nonnewton. Fluid Mech. 158 (2009) 85–90.
[27] R. Benzi, T. Divoux, C. Barentin, S. Manneville, M. Sbragaglia, F. Toschi, Continuum modeling of shear startup in soft glassy materials, Phys. Rev. E 104 (3) (2021).
[28] M. Jalaal, N.J. Balmforth, B. Stoeber, Slip of spreading viscoplastic droplets, Langmuir 31 (44) (2015) 12071–12075.
[29] G. Martouzet, L. Jorgensen, Y. Pelet, A.L. Biance, C. Barentin, Dynamic arrest during the spreading of a yield stress fluid drop, Phys. Rev. Fluids 6 (4) (2021).
[30] M. Jalaal, B. Stoeber, N.J. Balmforth, Spreading of viscoplastic droplets, J. Fluid Mech. 914 (2021) A21.
[31] M. Kim, E. Lee, D. Kim, R. Kwak, Decoupled rolling, sliding and sticking of a viscoplastic drop on a superhydrophobic surface, J. Fluid Mech. 908 (2021) A41.
[32] L. Rapoport, B.R. Solomon, K.K. Varanasi, Mobility of Yield Stress Fluids on Lubricant-Impregnated Surfaces, ACS Appl. Mater. Interfaces 11 (17) (2019) 16123–16129.
[33] A. Wixforth, C. Strobl, C. Gauer, A. Toegl, J. Scriba, Z. von Guttenberg, Acoustic manipulation of small droplets, Anal. Bioanal. Chem. 379 (2004) 982–991.
[34] T.A. Waigh, Microrheology of complex fluids, Rep. Prog. Phys. 68 (3) (2005) 685–742.
[35] V. Vitali, G. Nava, A. Corno, M. Pezzotti, F. Bragheri, P. Paie, R. Osellame, M. A. Ortenzi, I. Cristiani, P. Minzioni, T. Bellini, G. Zanchetta, Yield stress “in a flash”: investigation of nonlinearity and yielding in soft materials with an optofluidic microrheometer, Soft Matter 17 (2021) 3105–3112.
[36] P. Edera, M. Brizioli, G. Zanchetta, G. Petekidis, F. Giavazzi, R. Cerbino, Deformation profiles and microscopic dynamics of complex fluids during oscillatory shear experiments, Soft Matter 17 (2021) 8553–8566.
[37] D. Ferraro, M. Serra, D. Filippi, L. Zago, E. Guglielmin, M. Pierno, S. Descroix, J. L. Viovy, G. Mistura, Controlling the distance of highly confined droplets in a capillary by interfacial tension for merging on-demand, Lab Chip 19 (1) (2019) 136–146.
[38] S. Sett, X. Yan, G. Barac, L.W. Bolton, N. Miljkovic, Lubricant-Infused Surfaces for Low-Surface-Tension Fluids: Promise versus Reality, ACS Appl. Mater. Interfaces 9 (41) (2017) 36400–36408.
[39] M. Caggioni, V. Trappe, P.T. Spicer, Variations of the Herschel-Bulkley exponent reflecting contributions of the viscous continuous phase to the shear rate-dependent stress of soft glassy materials, J. Rheol. 64 (2) (2020) 413–422.
[40] C. Semprebon, S. Varagnolo, D. Filippi, L. Perlini, M. Pierno, M. Brinkmann, G. Mistura, Deviation of sliding drops at a chemical step, Soft Matter 12 (2016) 8268–8273.
[41] T. Toth, D. Ferraro, E. Chiarello, M. Pierno, G. Mistura, G. Bissacco, C. Semprebon, Suspension of water droplets on individual pillars, Langmuir 27 (8) (2011) 4742–4748.
[42] M.S. Sadullah, C. Semprebon, H. Kusumaatmaja, Drop Dynamics on Liquid-Infused Surfaces: The Role of the Lubricant Ridge, Langmuir 34 (27) (2018) 8112–8118.
[43] L. Mahadevan, Y. Pomeau, Rolling droplets, Phys. Fluids 11 (1999) 2449–2453.
[44] S.R. Hodges, O.E. Jensen, J.M. Rallison, Sliding, slipping and rolling: the sedimentation of a viscous drop down a gently inclined plane, J. Fluid Mech. 512 (2004) 95–131.
[45] B.M. Mognetti, H. Kusumaatmaja, J.M. Yeomans, Drop dynamics on hydrophobic and superhydrophobic surfaces, Faraday Discuss. 146 (2010) 153–165.
[46] S.P. Thampi, R. Adhikari, R. Govindarajan, Do Liquid Drops Roll or Slide on Inclined Surfaces? Langmuir 29 (10) (2013) 3339–3346.

[47] D. Richard, D. Quere, Viscous drops rolling on a tilted non-wettable solid, Europhys. Lett. 48 (3) (1999) 286–291.
[48] V. Lombardi, M. La Rocca, A. Montessori, S. Succi, P. Prestininzi, On the fate of a drop jumping over a gap, J. Fluid Mech. 949 (2022) A27.
[49] H.Y. Kim, H.J. Lee, B.H. Kang, Sliding of liquid drops down an inclined solid surface, J. Colloid Interface Sci. 247 (2) (2002) 372–380.
[50] N. Le Grand, A. Daerr, L. Limat, Shape and motion of drops sliding down an inclined plane, J. Fluid Mech. 541 (2005) 293–315.
[51] S. Varagnolo, D. Ferraro, P. Fantinel, M. Pierno, G. Mistura, G. Amati, L. Biferale, M. Sbragaglia, Stick-Slip Sliding of Water Drops on Chemically Heterogeneous Surfaces, Phys. Rev. Lett. 111 (2013), 066101.
[52] J. Pemeja, B. Geraud, C. Barentin, M. Le Merrer, Wall slip regimes in jammed suspensions of soft microgels, Phys. Rev. Fluids 4 (3) (2019).
[53] P. Saramito, A. Wachs, Progress in numerical simulation of yield stress fluid flows, Rheol. Acta 56 (2017) 211–230.
[54] T. Mouterde, P.S. Raux, C. Clanet, D. Quere, Superhydrophobic frictions, PNAS 116 (17) (2019) 8220–8223.
[55] P. Sarkiris, K. Ellinas, D. Gkiolas, D. Mathioulakis, E. Gogolides, Motion of drops with different viscosities on micro-nanotextured surfaces of varying topography and wetting properties, Adv. Funct. Mater. 29 (2019) 1902905.
[56] H. Xu, A. Clarke, J.P. Rothstein, R.J. Poole, Viscoelastic drops moving on hydrophilic and superhydrophobic surfaces, J. Colloid Interface Sci. 513 (2018) 53–61.